



# Generic comparison of ISM and LSIT interpretation of geo-resistivity technology data, using constraints of ground truths: a tool for efficient explorability of groundwater and related resources

Nyakno Jimmy George<sup>1</sup> · Kufre Richard Ekanem<sup>1</sup> · Aniekan Martin Ekanem<sup>1</sup> · Ndifreke Inyang Udosen<sup>1</sup> · Jewel Emem Thomas<sup>1</sup>

Received: 26 January 2022 / Accepted: 13 April 2022 / Published online: 18 May 2022

© The Author(s) under exclusive licence to Institute of Geophysics, Polish Academy of Sciences & Polish Academy of Sciences 2022

## Abstract

Geo-electrical resistivity technology, an investigative tool for prognosis or prospection of subsurface resources in relation to hydrogeology, environment, Archeology, engineering and mining, was employed to estimate the prime geo-electrical indices in a sedimentary environment using the interpretative candidacy of direct modelling of geo-electrical data through inverse slope method (ISM) and inverse modelling utilizing the least squares inversion technique (LSIT). The aim was to generically compare in-line with borehole indices, the results from the direct interpretation (ISM) with the conventional digitally computerized method (LSIT), which is associated with the ill-posed problem of inverse theory. The image maps, regression analysis and charts, from the qualitative and quantitative analyses of resistivity data, show that marginal correlations exist between ISM and LSIT in layer one while maximal correlation of resistivities is revealed in layers two and three. The curve types obtained from LSIT were 100% in agreement with the values of resistivities obtained from the ISM. Comparatively, the depth of investigation from the LSIT showcased a correlation with borehole depth in the range of 56.3–88.6% (average: 70.3%) while ISM has middling correlation of 79.0% with range of 68.0–87.7% in layers one to three distinctively delineated at the maximum electrical current separation. In terms of comparison, the depths and thicknesses displayed in Table 2 and Figs. 10–12, ISM is practically more compliant with the drilling results than the results from conventional and digitally computerized method (LSIT). Again, the results indicate the ill-posed problem of inverse theory associated with LSIT can be made well-posed by hybridizing the ISM and LSIT techniques in the interpretation of geo-resistivity data, mostly in the areas where there are no borehole logs (ground truths).

**Keywords** Geo-electrical resistivity technology · Inverse and forward modelling · ISM · LSIT · Nash–Sutcliffe optimization criterion

## Introduction

Geo-electrical resistivity technology, which deploys vertical electrical sounding (VES) and electrical resistivity tomography (ERT), has been employed by many authors in shallow/intermediate depth investigation for purposes such as hydrogeology, environment, archeology,

engineering and mining surveys (Bandani 2011; Ibanga and George 2016; Mohammed et al. 2021; Ekanem et al. 2022; Ikpe et al. 2022). The direct current inverse resistivity problem is usually ill-posed with respect to incompleteness and uncertainties in datasets. In an attempt to make the solution well-posed, regularization schemes must be incorporated in the inverse problem to find a unique and stable solution (Binley et al. 1995; Udosen and George 2018a). Although regularization plays a substantial role in the problem of inverse theory, there is a vast ambiguity in choosing the regularization schemes (Ghanati et al. 2021). In view of the attendant ambiguity in inverse model and the imagined effect on its applications, mostly when it is used alone in the area with no ground truthing information, integrated methodologies

---

Edited by Dr. Michael Nones (CO-EDITOR-IN-CHIEF).

---

✉ Nyakno Jimmy George  
nyaknojimmyg@gmail.com; nyaknogeorge@aksu.edu.ng

<sup>1</sup> Department of Physics (Geophysics Research Group), Akwa Ibom State University, Mkpatt Enin, PMB 1162, Uyo, Nigeria

such as direct (ISM) technique are needed. Variability of resistivity in the subsurface is often viewed to take a nonlinear dimension during the numerically iterative techniques of least squares inversion or during the process of finding the resistivity model with goodness of fits in the entire sequence of quadrupole measurements of apparent resistivities (Tripp et al. 1984). In minimizing the ambiguity in measurements, real resistivities are often considered when referring to the unknown reality. Computed resistivities were assumed when referring to resistivities resulting from inversion and apparent resistivities are construed when both real and computed resistivities unfold the ones resulting from direct voltage measurements of assumed homogeneous media. In electrical resistivity measurement technology, vertical electrical sounding (VES) and electrical resistivity tomography (ERT) are ill-posed/ill-constrained or underdetermined inverse problems in as much as their solutions may be unstable or non-unique. Based on this realization, it is often ideal to couple the interpretation of VES and ERT data with depth dependent geological equivalence in areas where these geological data are available. Besides, the geological data of the subsurface are localized and the deductions may not be a generalized solution for areas that are remote from the sources of geological information. Therefore, comparison, calibration, validation and correlation of methodologies in phenomenological interpretation of non-unique geo-resistivity data are imperative for results that are believed to be geologically consistent in small and large scale geophysical and geological measurements. As a good practice, applying two or more complementary methods of interpretation in many a time can reduce the high degree non-uniqueness. Despite verifying the efficacy of the inverse slope method (ISM) for the interpretation of electrical sounding data in order to determine the primary geo-electric indices, the main aim of this research is to compare the direct/forward modelling with the ill-posed iterative inversion (inverse modelling), which relies on the mathematically theoretical curves to generate the primary geo-electrical indices. In order to compare the interpretation of geo-electric data using the LSIT with the inverse gradient method or technique (ISM/IGT), ground truthing information were required as real data to see the degree of convergence/divergence of independent interpretations of VES data using ISM and LSIT. ISM has unique quality of generating earth resistivity indices without requiring theoretical models like the conventional inverse methods of curve matching do (Ghanati et al. 2021). Bouadou et al. (2019) opined that findings from field survey and laboratory experiment showcased that the inverse gradient method has the potential to be employed in VES data analysis acquired with any electrode array. This unique quality is

not accessible with all the other conventional analytical procedures that are currently in use.

## Description of the site of study, geology and hydrogeological conditions

### Study location

The study area is a sedimentary environment, located in a medium-sized newly designed residential estate, known and referred to as *Shelter Afrique* in Akwa Ibom State, southern Nigeria. The referred study area was spatially geo-referenced and the coordinates transformed from degree to meters. This was done by finding the respective latitude and longitude difference from their respective common reference points and multiplying them by 111,139 m. The resulting coordinates in meters were used for kriging. The survey area is positioned in the mid-western part of Akwa Ibom State in southern Nigeria. It massively cuts across Ibesikpo County in the south; with a small portion of the area located in Uyo, the headquarters of Akwa Ibom state (Fig. 1). The inhabiting landmass, which is landlocked outspreads between latitudes  $4.958^{\circ}$  and  $4.9917^{\circ}$  N and longitudes  $7.9417^{\circ}$  and  $7.9750^{\circ}$  E, with an area that is about  $31 \text{ km}^2$ . The area is a table land that is currently witnessing new dwellers and new state-of-the-art structures. It is also characterized by good road network and buildings that are well-planned to give room for long VES traverses. The climate is semi-temperate with scrubs. The study area witnesses dry and wet seasons. The wet season begins in earnest from April to September and dry season starts from October to March. The temperature ranges from  $26$  to  $32^{\circ}$  C while its annual rainfall range is from  $2.0$  and  $2.5$  m. The entire catchment is drained by the tributaries of Enyiong Creek, which is the main perennial reservoir of surface water in Itu Local Government Area (Ibuot et al. 2013; Ekanem et al. 2019; Uwa et al. 2019; George 2021).

### Geology and hydrogeological settings

The Youngest Continental Plain sand/Benin Formation of the Niger Delta of southern Nigeria is where aquifer systems in the study area are located and subsurface water is drilled at various depths from this formation. The Benin Formation is characteristically noted by many researchers to be inundated with intercalations of pockets of arenites and slight/petty argillites (Peters 1982, 1989; Obianwu et al. 2011; George et al. 2014; Akpan et al. 2013; George et al. 2017). The Agbada and Akata Formation, respectively, lie below the Benin Formation in

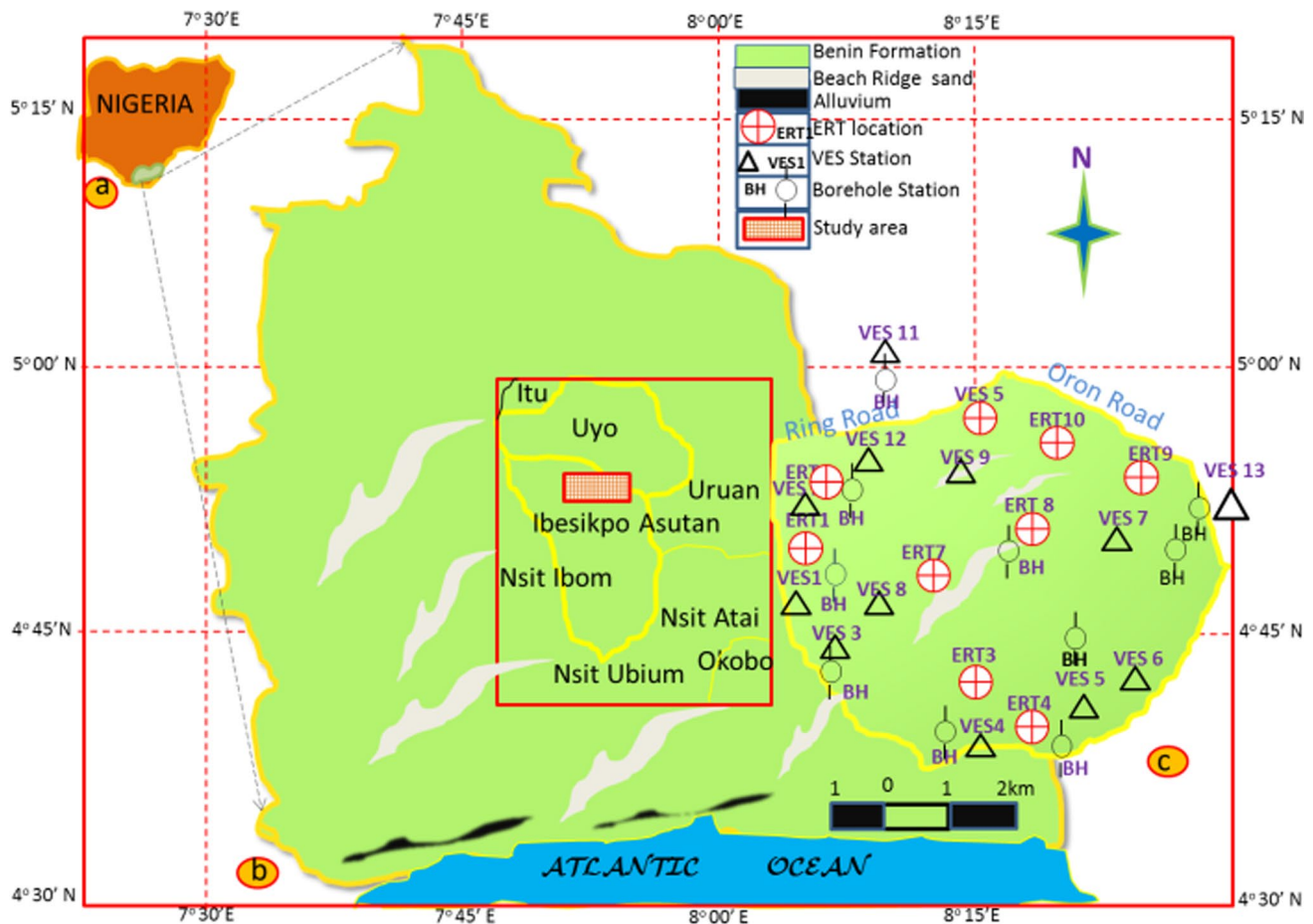


**Fig. 1** a Schematic map of Nigeria showing the geographic location of Akwa Ibom State in Southern Nigeria b map of Akwa Ibom State showing Atlantic Ocean and the geographical settings of the study

area, c geographic and model domain map showing geology, VES and ERT points and Borehole locations

chronological depths of burial (Peters 1982, 1989). The study area explicitly, fits grossly into the Benin Formation and somewhat into the Beach Ridge Complex and Alluvium of Quaternary Period as Fig. 1 depicts. The constituents of Benin Formation preponderantly range from fine to gravelly sands (Fig. 2) and by composition; the light grey complementary petty argillites are comparatively insignificant and occasionally strewn. Morphological disparities caused by deposition, sedimentation and erosion are occasionally observed on the shallowest planes after downpour (Thomas et al. 2020). The deposits of sedimentary constituents are regularly observed in the dipping altitude and they are appealing to the gravitational attraction. The grayish muddy sand grains have a characteristic texture that varies from finer to coarsening textures and they are sequentially intercalating in nature according to Short and Stauble (1965). Myriad geological dynamics regulate the economic availability of groundwater and the depth of burial of aquifer in the survey area. According

to Tizro (2012), some of these dynamics include—the stratigraphical disturbances and geological sequence of hydrogeological units. The hydraulic networks between seasonal drawdown and subsurface water level or groundwater conduit topography regulate the bathymetry of water wells in the study area (Ekanem et al. 2022).

## Material and methods

### VES and ERT measurements

The geo-electrical resistivity technology, which ensures electrical sounding or electrical drilling, is soil conductivity—sensitive tool that maintains current and potential electrodes along a straight path at the equivalent relative spacing around a fixed central position and it is frequently deployed in the hydrogeological and solid mineral explorations (Akpan et al. 2018; Ibuot et al. 2019; Ekanem et al.

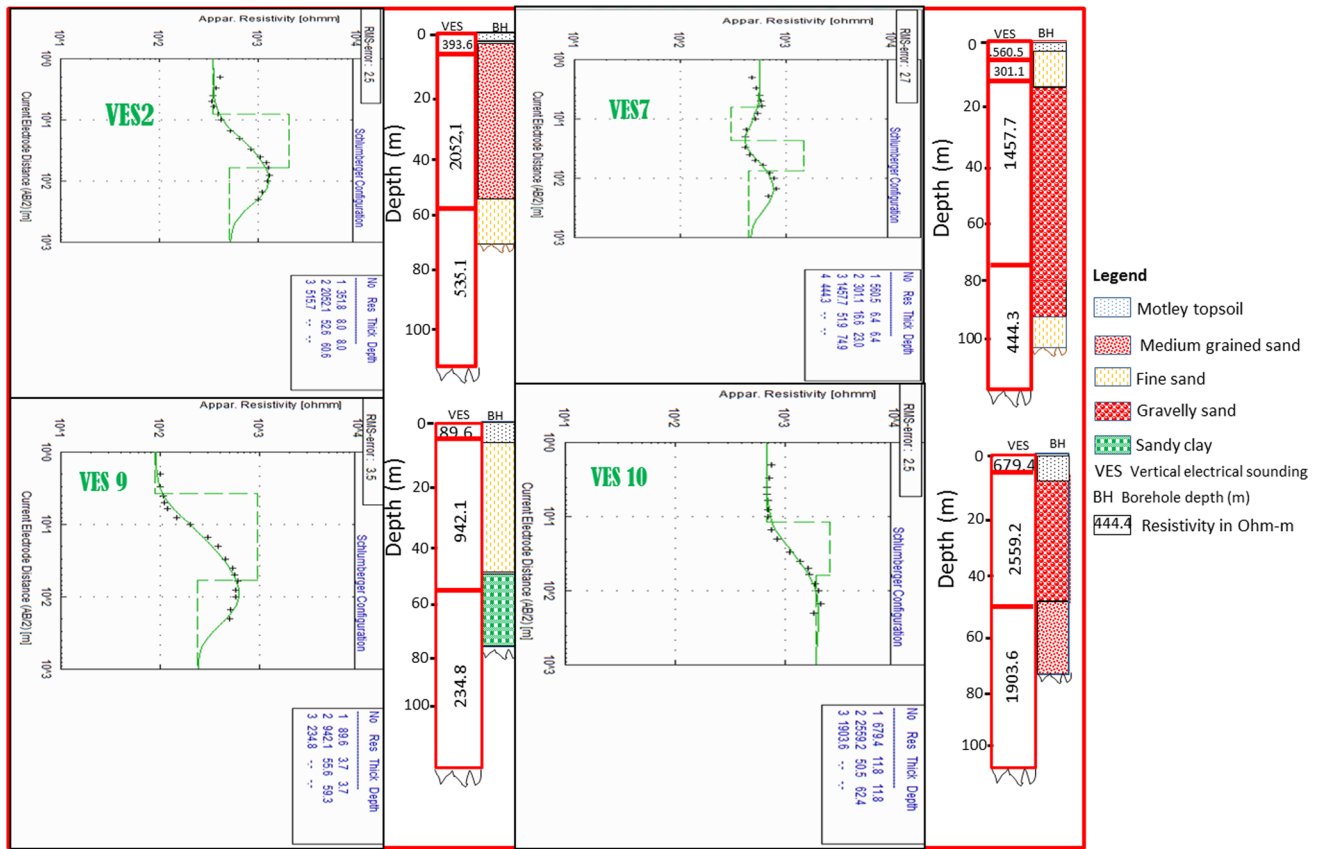


**Fig. 2** Sampled correlations of VES 2, 7, 9 and 10 curves with their adjoining lithological log in the study area

2021). Geo-sounding resistivity technicality deployed in this work involves a one-dimensional vertical electrical sounding (VES) and two-dimensional electrical resistivity tomography (ERT). These techniques were performed adjacent to water wells through the deployment of IGIS signal enhancement resistivity meter (SSP-MP-ATS) and its fittings in the area surveyed. Thirteen (13) and ten (10) closely spaced VES and ERT points, adjacent to water boreholes were, respectively, sounded (see Fig. 1). The procedure used in VES data acquisition was Schlumberger configuration with maximum current electrode separations (AB) of 400 m. Again, the ERT, leading to 2-D data acquisition used the Wenner electrode configuration with spread length of 105 m, taking through 5 m separations (Thomas et al. 2020). All the precautionary measures opined by Zohdy et al. (1974), Zohdy 1989; Evans and George 2007; Akpan et al. (2013) were observed for quality assurance. The apparent resistance of the earth for Schlumberger and Wenner techniques was determined as  $R_{as}$  and  $R_{aw}$ , respectively, for the VES and ERT technique. For VES and ERT methods, the apparent resistivities  $\rho_{as}$  and  $\rho_{aw}$  were computed using the equations given below:

$$\rho_{as} = \pi \cdot \left[ \frac{(AB/2)^2 - (MN/2)^2}{MN} \right] \cdot R_{as} \quad (1)$$

$$\rho_{aw} = 2\pi a R_{aw}, \quad (2)$$

where AB, MN and  $a$  are, respectively, electrical current electrode spacing, separation of potential electrodes and Wenner electrode spacings. The term on the right hand side is obtained by multiplying the  $R_{as}$  and  $R_{aw}$  by the geometric factor for Schlumberger and Wenner electrode configurations, respectively, in order to obtain the apparent resistivities  $\rho_{as}$  and  $\rho_{aw}$  for both the Schlumberger and Wenner spacing configurations in Eqs. 1 and 2, respectively. On a logarithmic scale, apparent resistivities were plotted manually against half of the current electrode spacings. Smoothing was performed on the data by removing the spurious signatures (outliers) that did not follow the prevailing curve trend entrenched by the geology of the layers that current passed through. The smoothed, VES apparent resistivities were interpreted further in two ways. The computer modeling least squares inversion technique (LSIT), which, according to Oladapo et al. (2004) and Obiora et al. (2015); George

(2020) used the data to generate the final curves by comparing the field curves to the existing theoretical curves (Fig. 2). This was possible using a RESIST code developed by Vander Velpen and Sporry (1993). The field data were reduced to their geologically consistent equivalent models using computer-modeling techniques (Zohdy et al. 1974). Following a couple of iterations, a reasonably acceptable disparity observed between the field and theoretical data were obtained through absolute root-mean-square (RMS) error, which was generically found to be less than 10% (Fig. 2). For ERT, involving a two-dimensional (2D) inversion, RES2DINV software program was used and the same iterations in VES was applied until a reasonable RMSE indicating a good fit between the theoretical and field data were achieved (Loke and Barker 1996; Loke and Dalhin 2002; Loke et al. 2003). The inverse gradient method (ISM) (Kouassi et al. 2017; Bouadou et al. 2019), which applied direct/forward technique to predict the primary geo-electric indices in Fig. 3. In case 1, the curves were electronically deciphered quantitatively through a 1-D least squares computer-aided software program, known as WINRESIST (Vander Velpen and Sporry 1993) with the constraints of nearby mechanically logged borehole indices. The software program supplied details of the interpreted curve by delineating the primary geo-electric indices such as depth, layer resistivity, thickness and the root-mean-squares error (RMSE) (generally < 10%). The RMSE describes the degree of goodness of fit between the theoretical curve and the curve from the field data (see Fig. 2). Also, by inversion of apparent resistivities computed from Eq. 2, using RES2DINV VER 3.59 Geotomo software code, theorized by Loke and Barker (1996), Loke and Dalhin (2002) and Loke et al. (2003), the ERT images (Fig. 4) were modelled after preparing the separation and the apparent resistivity values in tandem with the RES2DINV VER. 3.59 Geotomo software format. The software package generated a resistivity model of the shallow subsurface

based on iterative smoothness-constrained least squares, replicated on the resulting electrical resistivity tomography (Fig. 4). The inverse gradient method (ISM), theorized by Sankarnaryan and Ramanujachary (1967) for the analyses and interpretations of Wenner array compliant geo-sounding data or the Schlumberger method is used to generically compare, validate and calibrate VES and ERT data mostly when there is no borehole information, by applying the field equation to directly obtain the resistivities and thicknesses of the subsurface layers from the field datasets (Asfahani 2016; Bouadou et al. 2019). The method in Wenner array plots the inverse of resistance against the constant electrode separation ( $a$ ) such that the number of linear segments identified on the graph corresponds to the number of layers the injected current penetrated. The inverse of the slope of each segment of the graph gives the true resistivity of the layer while the respective intersections of the segments give the depth of each of the layers. In Schlumberger array, ISM was deployed in VES data interpretation by plotting the ratio of half of current electrode separation to apparent resistivity ( $\frac{AB}{2}/\rho_a$ ) against half of current Bouadou et al. (2019). Electrode separations ( $\frac{AB}{2}$ ) as developed by Asfahani (2016), Kouassi et al. (2017) and each sounding station generates a graph with linear segments corresponding to the number of layers as showcased by Fig. 5. The ISM results in Fig. 3 show that the last segment on all the interpreted VES is characterized by a low or near negative slopes, which indicate the presence of a very high resistivity layer.

The values of inverse of the slopes of the various segments were equaled to the true resistivity of the corresponding strata while the thicknesses were deduced from the intersections of the segments. The true resistivity of the layers was evaluated by Eq. (3):

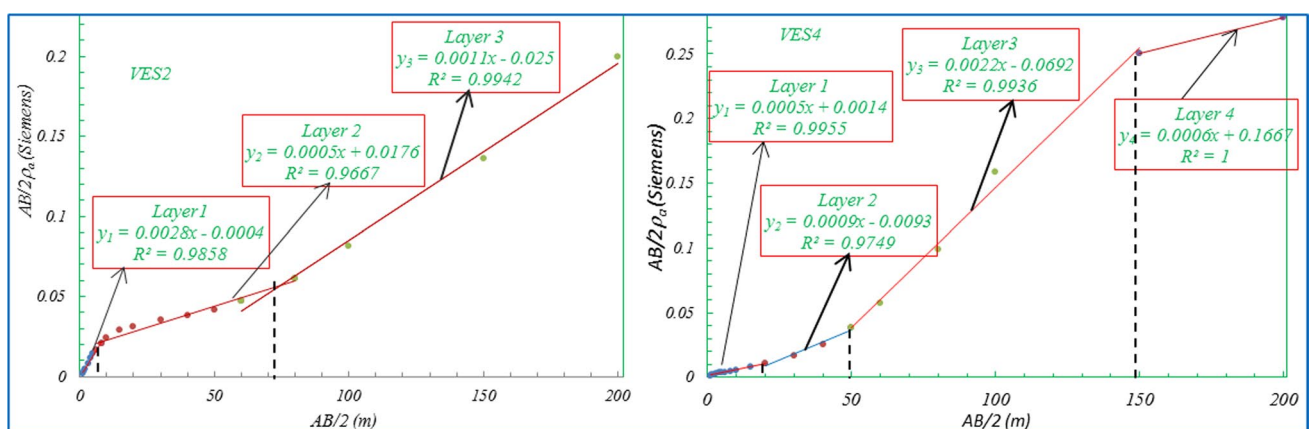


**Fig. 3** Samples of VES interpretation by IGM at VES points 2 and 4 showing the linear segments and their equations leading to the determination of different primary geo-electric indices (resistivity, thickness and depths)

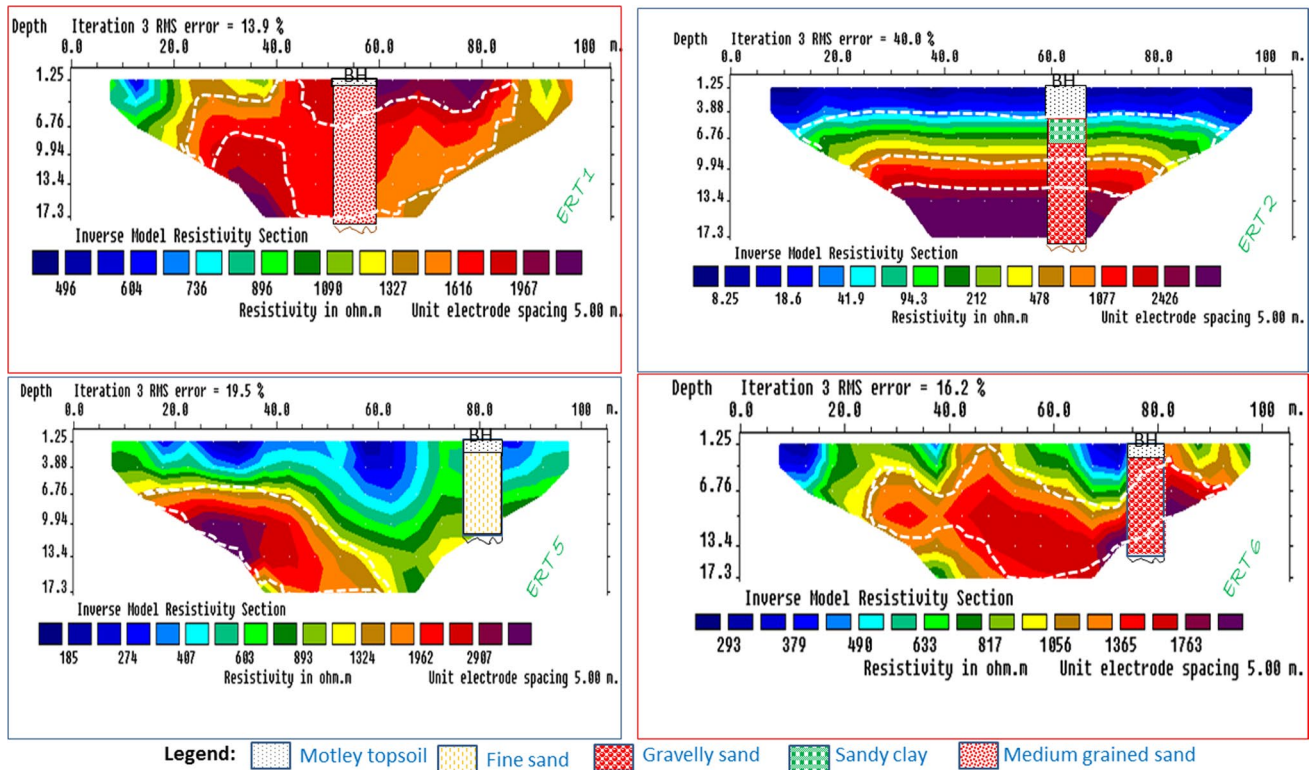
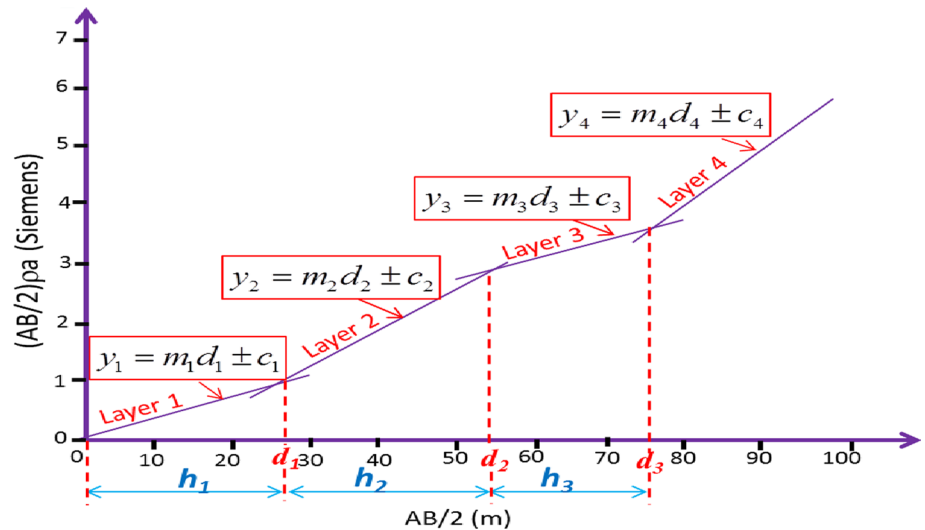


Fig. 4 Representatives of ERTs 1, 2, 5 and 6 with their adjoining lithological log in the study area

Fig. 5 Sketch showing a plot of ratio of AB/2 to apparent resistivity against AB/2 for ISM in Schlumberger array



$$\rho_n = \frac{1}{|m_i|}, \tag{3}$$

where  $m_i$  is the gradient of the  $i$ th linear segment and  $i = 1, 2, 3, \dots, n$  and  $n$  is the deepest layer number assessed by the current at the maximum current electrode separation. The depth ( $d$ ) to the different boundaries was obtainable generally by the use of intercept-slope relation in Eq. (4):

$$d_i = \frac{2(c_{i+1} - c_i)}{3(m_i - m_{i+1})}, \tag{4}$$

where  $m$  and  $c$  are the corresponding slopes and intercepts of the linear segments while  $i$  is the number of segments ( $i = 1, 2, 3, \dots$ ), which corresponds to the number of strata. The thickness of each layer ( $h$ ) is defined as the difference

between the depths of two consecutive strata and at the point of intersection,  $y_1 = y_2$  according to Fig. 5. As opined by Sanjiv (2010) and Bouadou et al. (2019), the intersections of the projected segments on the  $x$ -axis multiplied by a factor  $2/3$  give the true depth of the interfaces. Practically according to Bouadou et al. (2019), in the first segment, the value of the first thickness of the layer is equivalent to the value of the first intersection of the projected segments on the  $x$ -axis. Each line segment represents a layer and the intersections of the line segments, multiplied by a factor of  $2/3$ , correspond to the depths of the particular layers. The ISM was identified with ease of interpretation of surface resistivity data as standard curves, partial and total curve matching were not required but the results were often characterized by reasonably good results (Bouadou et al. 2019). With the combination of the inverse modelling technique (LSIT) and direct modelling technique within the vicinity of mechanically drilled borehole data, the calibration of direct and inverse VES interpretation techniques were assessed and the primary geo-electric indices determined independently from the ISM and LSIT techniques as given in Table 1.

## Results

### Results

Employing the techniques of LSIT and ISM independently in VES interpretation, the qualitative and quantitative results in Table 1 show similar trend. Qualitatively, the curve type in both ISM and LSIT at VESs 1, 2, 8, 9, 10 and 12 is  $H$  with 46.1% composition. At VESs 3, 4, 5 and 13, the curve types are, respectively,  $AK$  and  $HK$  at 15.4% composition in each pair while curve type  $AH$  (VES 4),  $KQ$  (VES 6) and  $A$  (VES 11), respectively, has 7.7% each. Quantitatively, Table 1 shows the summary of primary geo-electric indices for the thirteen VES points, which show a strongly similar trend for the two techniques independently used in VES interpretations. The similarity in trend is demonstrated in the uniformity of curve types in the two techniques. The ERT results (Fig. 4) also correlate fairly with the logged boreholes and VES results. The marginal disparities between geo-electric results and geology are in agreement with the conclusion by Tomitope and Adeniyi (2016) that geo-electric sections are not totally in tandem with geologic sections. As the major preoccupation of this research, the most probable correlation with the nearby borehole is of paramount concern in comparing, calibrating or validating the results interpreted independently between ISM and LSIT. The results in Table 1 are used in generating the correlations of the earth's consistent resistivities for the defined layers in ISM and LSIT that current passed through during geo-electric sounding as revealed in Fig. 6. The primary geo-electric indices (layer

resistivities, thickness and depth) measured at various coordinate locations of the study area are apt as the basis of comparison and possible calibrations of ISM and LSIT. The independent joint interpretation of layered resistivities, depths and thickness from ERT, ISM and LSIT have also resulted in some noticeable pattern recognition images (Figs. 4, 6, 7, 8 and 9) and charts in Figs. 10, 11, and 12. These aimed at making comparison, calibration and possible validation of interpretation of the ill-posed problem of geo-electrical resistivity data standardized.

### Nash–Sutcliffe optimization criterion model efficiency coefficient (NSOCMEC)

The variational depths were estimated from the interpretation of electric sounding data by the ISM and LSIT. These estimated depths were regarded as calculated/model depths ( $M_{Di}$ ) while the depth deduced from lithological logs were regarded as observed depths ( $O_{Di}$ ). The mean depth of the observed was estimated as ( $M_{DOi}$ ). The results of the calculated/modelled depth of geologic units penetrated by injected currents can be compared with the depths from drilling logs in order to verify the degree of reliability of ISM and LSIT using Nash–Sutcliffe optimization criterion model efficiency coefficient (NSOCMEC), given as one minus the ratio of error variance of a model values to the variance of the observed values and is mathematically expressed in percentage as:

$$\text{NSOCMEC} = \left[ 1 - \frac{\sum_{i=1}^n (O_{Di} - M_{Di})^2}{\sum_{i=1}^n (O_{Di} - M_{DOi})^2} \right] \times 100. \quad (5)$$

According to Yao et al. (2007), the optimization by NSOCMEC is judged according to the percentage ranges of values given below:

- Nash  $\geq 90\%$ : the model is excellent;
- $80\% < \text{Nash} < 90\%$ : the model is very satisfactory;
- $60\% < \text{Nash} < 80\%$ : the model is satisfactory;
- Nash  $< 60\%$ : the model is bad.

Since the model uses depth as the criterion for optimization between the modelled and the calculated values, it is considered efficient when the calculated/modelled depths are close to the observed depth, i.e., to say when the value of the NSOCMEC is close to 100%.

Moreover, to assess the potential effect of extreme values caused by sup-optimal results caused by datasets with large outliers, re-scaling of NSOCMEC is necessary in order to obtain the normalized NSOCMEC (NNSOCMEC), which is given by Eq. (6):

**Table 1** Summary of VES interpretation from ISM and LSIT at various VES stations

VES no	Location name	Coordinates		No. of layers	Primary geo-electric indices for ISM/LSIT						Lithological description
		Easting (m)	Northing (m)		Resistivity ( $\Omega\text{m}$ )		Thickness (m)		Depth (m)		
					ISM	LSIT	ISM	LSIT	ISM	LSIT	
1	ImohIta	168.6131	599.3582	3	500.0	393.6	0.9	1.8	0.9	1.8	Motley topsoil
					1666.7	1793.8	48.8	58.1	49.7	59.9	Medium grained sand
					714.3	535.1	–	–	–	–	Fine sand
2	Murray avenue	182.134	860.7621	3	357.1	351.8	5.2	8.0	5.2	8.0	Motley topsoil
					2000.0	2052.1	42.1	52.6	47.3	60.6	Gravelly sand
					909.1	515.7	–	–	–	–	Fine sand
3	Ambassador UbokUdom	19.0346	366.7587	4	833.3	1234.4	6.7	1.2	5.3	1.2	Motley topsoil
					1000.0	779.9	1.4	7.8	6.7	9.1	Fine sand
					1666.7	2301.8	64.4	48.2	69.7	57.3	Gravelly sand
					265.0	542.2	–	–	–	–	Fine sand
4	KufreEkanem Crescent	637.3368	30.05891	4	2000.0	996.3	17.8	1.5	17.8	1.5	–
					1111.1	2591.8	22.5	23.4	40.3	24.9	–
					454.6	472.5	58.0	46.8	98.3	71.8	–
					1666.7	1064	–	–	–	–	–
5	GodswillAkpabio Crescent 4	1110.567	166.6911	4	1428.6	1464.2	6.0	5.9	6.0	5.9	Motley topsoil
					833.3	411.9	33.9	19.3	39.9	25.2	Fine sand
					2000.0	2281.1	60.3	41.7	100.2	67.0	Gravelly sand
					625.0	867.1	–	–	–	–	Fine sand
6	UdoUdoma street	1263.803	234.2954	3	172.4	187.6	2.5	3.6	2.5	3.6	–
					2500.0	2109.9	63.8	72.4	66.2	76.0	–
					1428.6	1220.7	–	–	–	–	–
7	Alison Attah	1331.408	739.0743	4	454.5	1121.1	4.3	7.6	4.3	7.6	Motley topsoil
					555.6	427.1	13.0	15.0	17.3	22.6	Fine sand
					1428.6	2205.0	92.7	58.1	110.0	80.7	Medium grained sand
					625.0	1194.6	–	–	–	–	Fine sand
8	Chris Ekpenyong	497.6209	531.0754	3	400.0	294.2	11.1	11.3	11.1	11.3	Motley topsoil
					2000.0	2085.8	51.8	50.2	62.9	61.5	Gravelly sand
					714.3	323.0	–	–	–	–	Sandy clayey sand
9	Akpan Hogan Ekpo avenue	740.9964	1041.04	3	67.6	89.6	1.8	3.6	1.8	3.6	Clayey topsoil
					909.1	942.1	50.1	55.6	51.9	59.3	Fine sand
					454.4	234.8	–	–	–	–	Sandy clayey sand
10	Justice Edet Robert	502.1278	1072.589	3	833.3	679.4	11.6	11.8	11.6	11.8	Fine sand
					3333.3	2559.2	56.0	50.5	67.6	62.4	Gravelly sand
					1666.7	1903.6	–	–	–	–	Medium grained sand



Table 1 (continued)

VES no	Location name	Coordinates		No. of layers	Primary geo-electric indices for ISM/LSIT						Lithological description
		Easting (m)	Northing (m)		Resistivity (Ωm)		Thickness (m)		Depth (m)		
					ISM	LSIT	ISM	LSIT	ISM	LSIT	
11	EngrAtaayoEkwere	276.7801	1463.714	3	333.3	211.8	0.4	1.2	0.4/1.2	-	Clayey topsoil
					1111.1	1255.5	58.8	73.0	59.2	74.1	Fine sand
12	Dan Udofia avenue	299.3148	1068.082	3	2500.0	1901.3	-	-	-	-	Gravelly sand
					588.2	436.5	2.4	3.2	2.4	3.2	-
					1666.7	1938.8	50.3	56.1	52.7	59.3	-
13	UduakUdoudoh avenue	1687.772	874.283	4	833.3	541.3	-	-	-	-	-
					1111.1	1409.0	1.5	1.5	1.5	1.5	Motley topsoil
					384.6	308.3	4.1	5.0	5.6	6.5	Sandy clayey sand
					1111.1	2197.0	55.6	53.8	61.3	60	Medium grained sand
					1000.0	736.1	-	-	-	-	Fine sand

$$NNSOCMEC = \frac{1}{2 - NSOCMEC} \tag{6}$$

Based on the realism, Eq. 6 indicates that at NSOCMEC = 1, NNSOCMEC corresponds 1. At NSOCMEC = 0, NNSOCMEC corresponds to 0.5 and at NSOCMEC = -∞, NNSOCMEC corresponds to zero. The apt re-scaling of the NSOCMEC in Eq. 6 allows for quick and easier understanding and utilization of the NSOCMEC measurement of parameter estimation schemes used in model calibration.

### Discussion of results

The quantitative (resistivity, thickness and depth) and qualitative (exact number of curves) results that are consistent when constrained with mechanical boreholes have been identified from the inverse (LSIT) and direct (ISM) techniques applied to interpret the VES data known to associate with ill-posed problems and non-unique interpretative results (Simms and Morgan 1992; Friedel 2003). For efficient delineation of subsurface resources, hybrid methods in phenomenological interpretation of non-unique geophysical techniques are apt for resourceful and result-oriented exploration that leads to a corresponding efficient exploitation of subsurface resources. The combination of ISM, which has the capacity to determine the different geo-electric layers while typifying their resistivities and true thicknesses, with LSIT through independent interpretation to compare and validate the interpretative results was aided by the borehole data. The quality of the curve types in the LSIT based on the resistivity trend in Table 1 is 100% in tandem with the trend in the ISM. The entrenched results show a trend that is marginally variable between the ISM and LSIT. Practically, the independent measurements of geo-electric indices from ISM and LSIT as shown in Table 2 show good match in the determined values of resistivities, depths and thicknesses for the layers that current passed through. For instance, the graphs in Fig. 6a–c indicate the respective ISM-LSIT plots of resistivities for layers 1–3 penetrated by current. The coefficients of determination for layers 1–3, respectively, give 73, 80.0 and 81% ISM-LSIT resistivity correlations for the regression lines generated from the plots (see Eqs. 7, 8, 9):

$$ISM = 0.8001LSIT + 152.53 \tag{7}$$

$$ISM = 0.8073LSIT + 271.18 \tag{8}$$

$$ISM = 0.5858LSIT + 472.15. \tag{9}$$

The slight variations in the correlation coefficients are in sync with the fact that fictitiousness of the subsurface medium decreases with depth due subsurface inhomogeneity (Zohdy et al. 1974). Generally, electrical resistivity measurements (VES and ERT) are often sensitive to

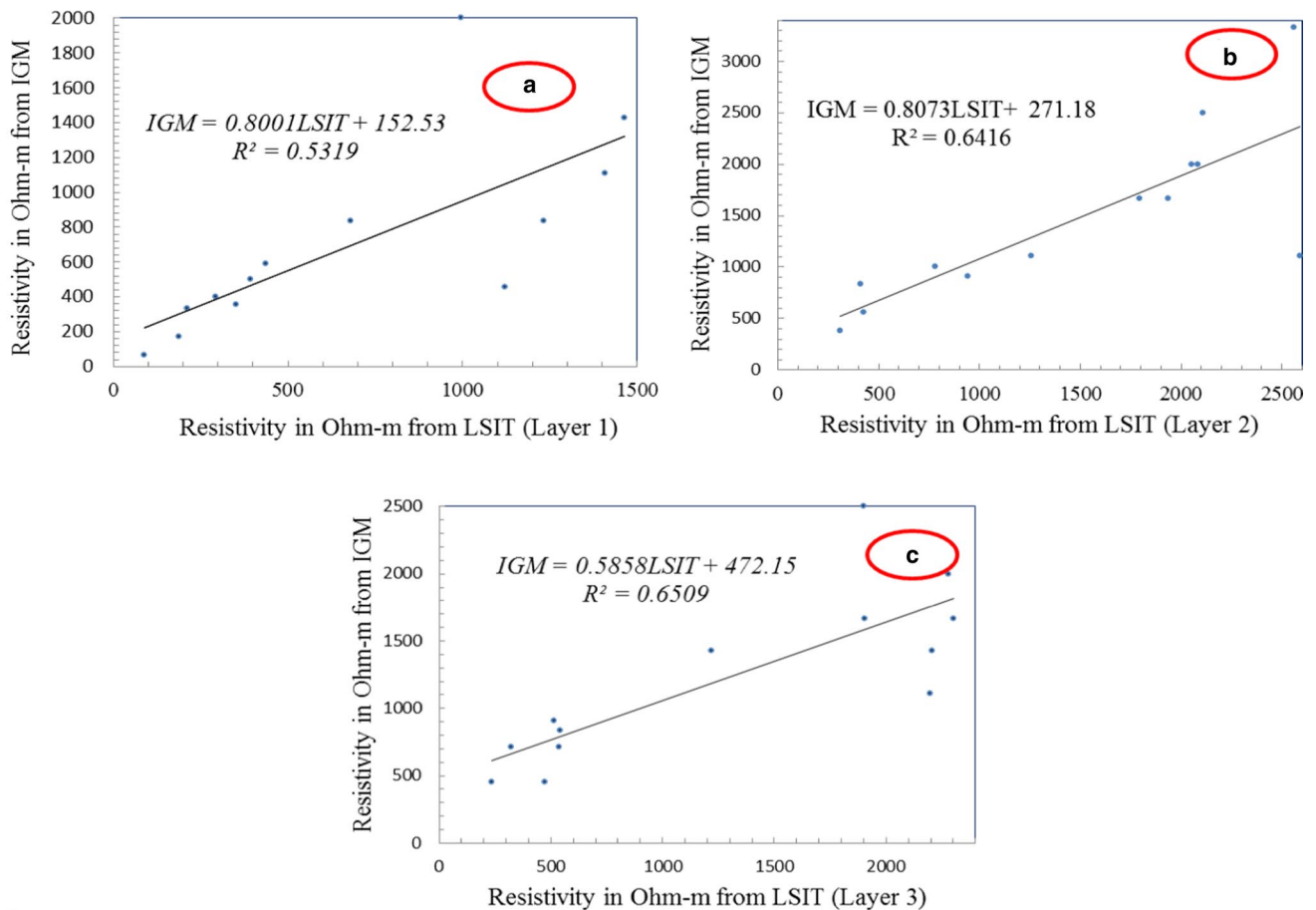
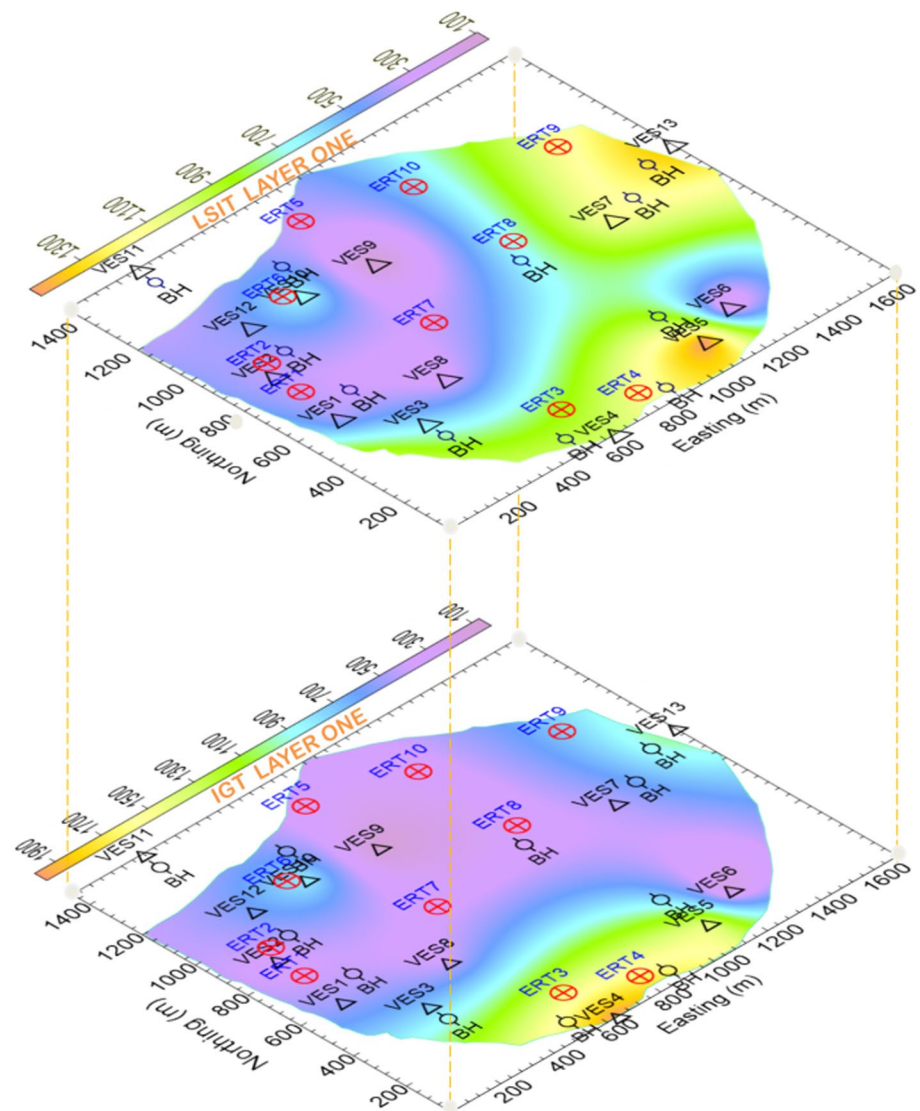


**Fig. 6** Graph showing IGM-LSIT plot for **a** layer one, **b** layer two and **c** layer three

electrode-spacing inaccuracies, potential errors as well as subsurface inhomogeneity (Mohammed et al. 2021). Interpreting resistivity data using inverse models (LSIT), which involve comparing the field data to theoretical data, will always have ambiguity except the interpretation is constrained with borehole data. In order to assess the level of goodness of fit, ISM technique was used to interpret the same data. Since the data were acquired closed to borehole, the two were compared to the borehole indices and the one with close fitness with the borehole data is regarded as the one that is less sensitive to the electrode-spacing errors, potential errors as well as subsurface inhomogeneity (Udosen and George 2018b; Mohammed et al. 2021). In terms of resistivities, Figs. 6, 7, and 8 showcase the resistivity pattern recognition for layers 1–3. Again, the uniformity or correlation of resistivity image gets better between LSIT and ISM with depth. However, the coarsening correlation in Fig. 6 (topmost layer) compared to the deeper layers is due to surface electrical effect caused by spurious effect of inhomogeneity in the interpretation of VES data using inverse and direct models. As resistivity inversion by numerical algorithms involves the minimization of error between the

observed apparent resistivity in order to obtain a good fit between the field data and the assumed theoretical model, interpreting LSIT without a borehole may be misleading as the technique is an ill-posed problem (Ghanati et al. 2021). Therefore, this pretext advances the reason while there must be variations between LSIT and ISM or ISM noticed as either significant or marginal variability in correlating the interpretive results from ISM and LSIT in Figs. 6, 7, and 8 and in Table 2. To assess the goodness of fit between the two candidates of VES interpretation, correlation were made between their depth and thickness results with nearby boreholes and the results show that ISM is more perfectly correlated with the borehole data than LSIT especially for layers 2 and three where the subsurface layer is stable and not fictitious (see Figs. 10, 11, and 12). As observed on Fig. 10, VES 4, 6 and 12 did not have the real logged data and this is why only two bars representing depths interpreted from ISM and LSIT techniques are, respectively, shown. However, in the rest of the VES points, additional one bar representing approximate depth from lithological logged borehole is added. The heights of the three bars clustered at each VES point correlate the closeness of depths obtained

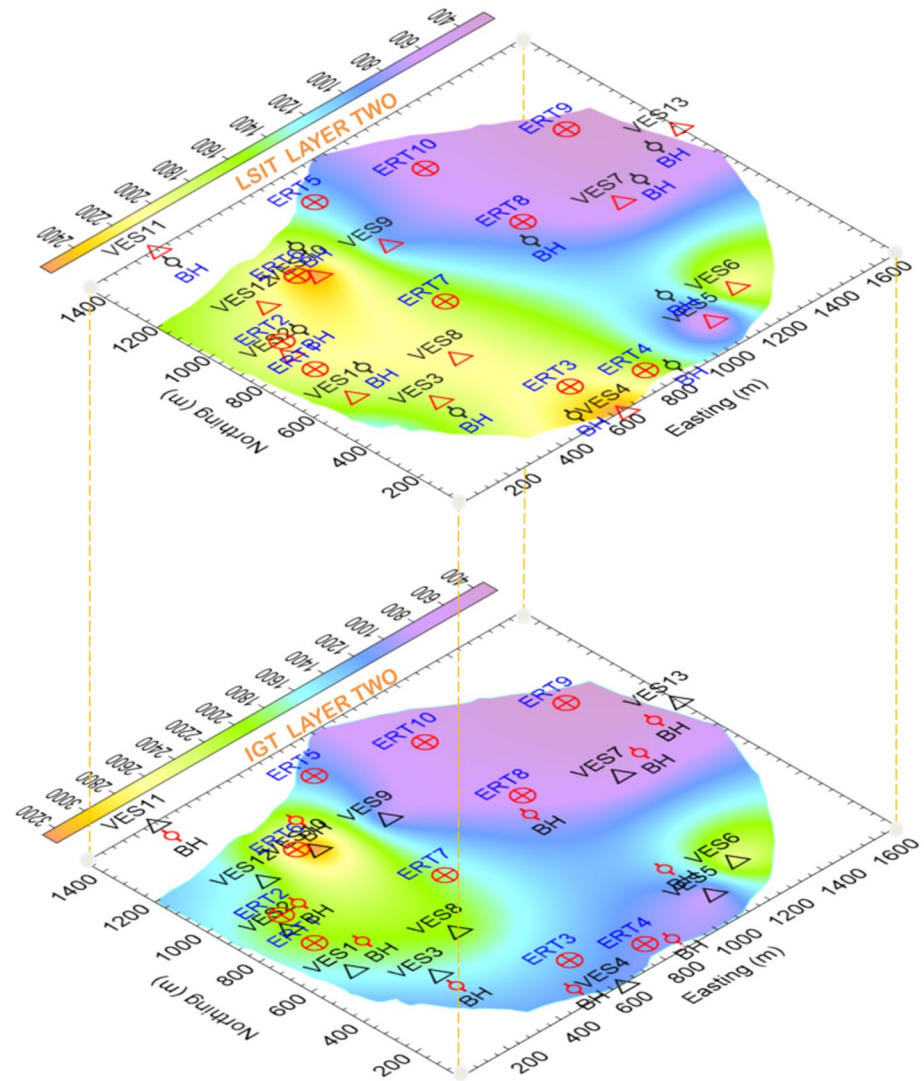
**Fig. 7** Comparison of resistivity image map of least-squares inversion technique (LSIT) and inverse slope technique (IGT) for layer one



from ISM and LSIT to the nearby approximate depth of borehole. In Figs. 11 and 12, the same diagrams are provided for layers 2 and 3. Based on these diagrams, the real drilling data are used as the reference point for validation/calibration of the methods (ISM and LSIT) employed. In Fig. 10, there are some spurious divergences of VES depths in layer one between ISM and LSIT while some convergences of depths between the two methods with respect to the nearby boreholes are also noticed. The same idea is also conveyed in Figs. 11 and 12 for layers 2 and 3. Although layer one (topmost) is often fictitious, the basis for spurious divergence of depth due to high degree of heterogeneity (Mohamed et al. 2014; George et al. 2015), layers two and three show extremely better harmonious convergence between ISM and borehole than LSIT, the traditional digital computerized method. As observed, the correlation amongst the primary geo-electric indices obtained from ISM and LSIT and even the drilling appears to be enhanced with

depth (see Figs. 7, 8, 9, 10, 11, and 12). The observed lithological logs (Table 1) from boreholes are quite in-line with the trend of resistivity values obtained near the borehole (Mohamed et al. 2014; Bouadou et al. 2019). According to the results in Table 2, the layer one resistivity values ranged from 67.6 to 2000.0  $\Omega m$  and 89.6–1464.2  $\Omega m$  with average values 2000.0  $\Omega m$  and 682.3  $\Omega m$ , respectively, for ISM and LSIT. In layer two, resistivity ranged 384.6–3333.3  $\Omega m$  and 308.3–2591.8  $\Omega m$  with average 1467.0  $\Omega m$  and 1481.3  $\Omega m$  for ISM and LSIT, respectively. Similarly, layer three interpreted by ISM and LSIT showed resistivity ranges of 454.4–2500.0  $\Omega m$  and 234.8–2301.8  $\Omega m$  with corresponding averages of 1221.7  $\Omega m$  and 1279.5  $\Omega m$ . In the VES identified with the fourth layer, resistivity spread between 256.0–1666.7  $\Omega m$  and 542.2–1194.6  $\Omega m$  with corresponding averages of 836.3  $\Omega m$  and 880.8  $\Omega m$ . The interpreted datasets showed corresponding ranges for layers 1–3 in ISM as 0.4–17.8 m, 5.6–67.6 m and 61.2–110.0 m depths penetrated

**Fig. 8** Comparison of resistivity image map of least-squares inversion technique (LSIT) and inverse gradient technique (IGT) for layer two



and 1.2–11.8 m, 6.5–76.0 m and 57.3–80.7 m, respectively, for layers 1–3 in the depth penetrated in LSIT. The ISM-LSIT depth averages for layers 1–3 are 5.4 m, 43.6 m and 87.9 m and 4.8 m, 46.3 m and 67.4 m, respectively. Similarly, the interpreted datasets showed corresponding thickness ranges for layers 1–3 in ISM as 0.4–17.8 m, 1.4–63.8 m and 55.6–92.7 m and thickness in LSIT as 1.2–11.8 m, 6.5–76.0 m and 57.3–80.7 m, respectively. In terms of averages, the ISM and LSIT showed thickness values of 5.6 m, 38.3 m and 66.2 m and 4.8 m, 41.5 m and 49.7 m, respectively. These ranges and mean values of interpreted primary geo-electric indices highlighted above indicate on the average, marginally enhanced depths and thicknesses from layer one to maximally enhanced depths in ISM (direct model) when compared to the conventional and digitally computerized method (LSIT) (see Table 2 and Figs. 10, 11, and 12). The analysis of the depth of penetration showed that the LSIT has correlation with borehole depth in the range of 56.3–88.6% (average: 70.3%) while ISM has average

correlation of 79.0% with range of 68.0–87.7% in layers 1–3 clearly delineated in this study. On the basis of the results of this analysis, ISM is marginally more compliant with the drilling data than the conventional and digitally computerized method (LSIT). This according to (Ghanati et al. 2021) may be due to the ambiguity in choosing the regularization schemes, in solving the inverse problem associated with the least squares inversion technique in the traditional digitally computerized method, which often requires a fit between the field data and the theoretical datasets. Since geo-electrical resistivity technology is used in hydrogeology, environment, archeology, engineering and mining surveys (Panda et al. 2017; Mohammed et al. 2021) to explore and exploit the geo-resources, techniques leading to efficient prediction of depths of investigation, lateral and transverse spreads of resources sought for, reproducibility, versatility and precision/sensitivity as well simplicity in usage are the characteristics to be considered, which are all found in ISM.

**Fig. 9** Comparison of resistivity image map of least-squares inversion technique (LSIT) and inverse gradient technique (IGT) for layer three

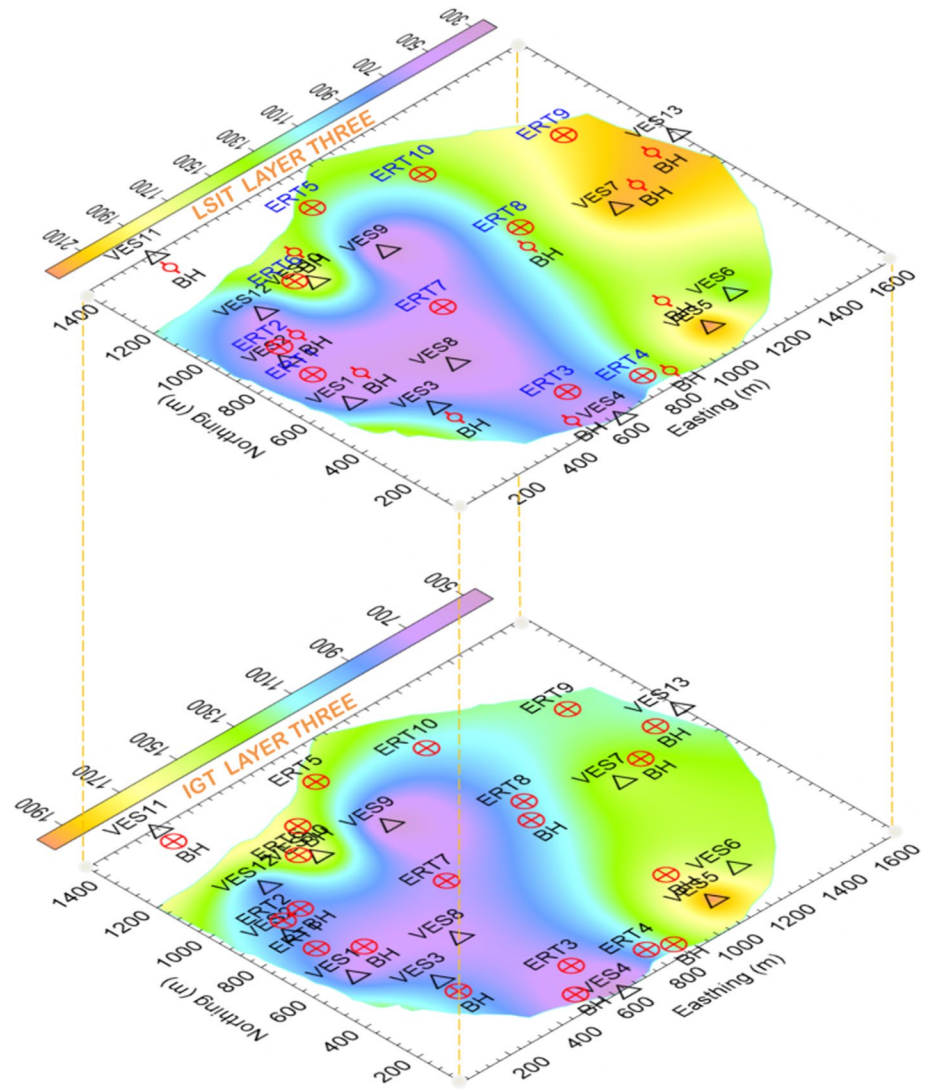


**Fig. 10** Delineated depth correlation of IGM and LSIT with approximate layer one depth from lithological data at different VES locations

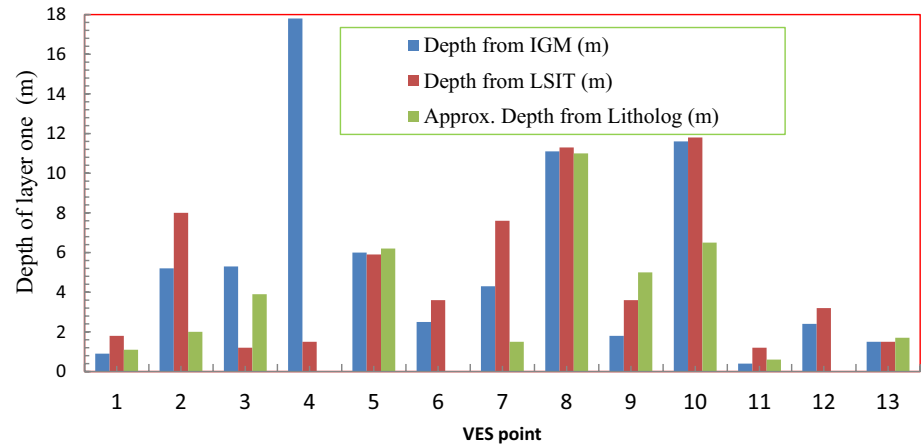


**Fig. 11** Delineated depth correlation of IGM and LSIT with approximate layer two depth from lithological data at different VES locations

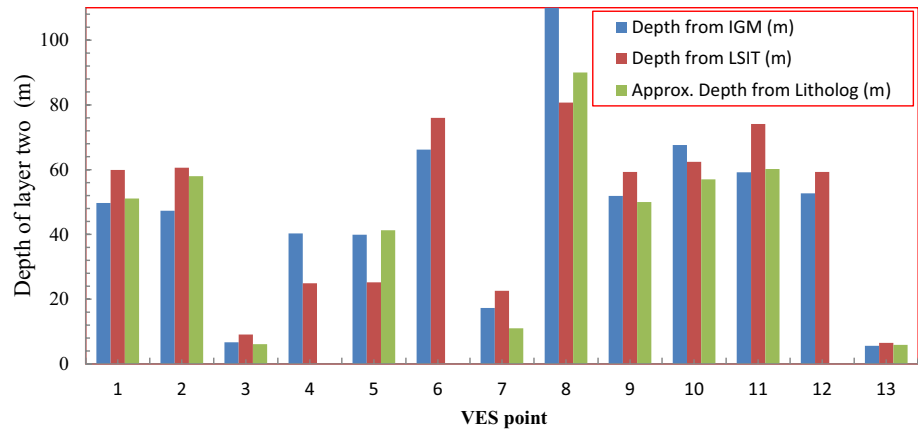
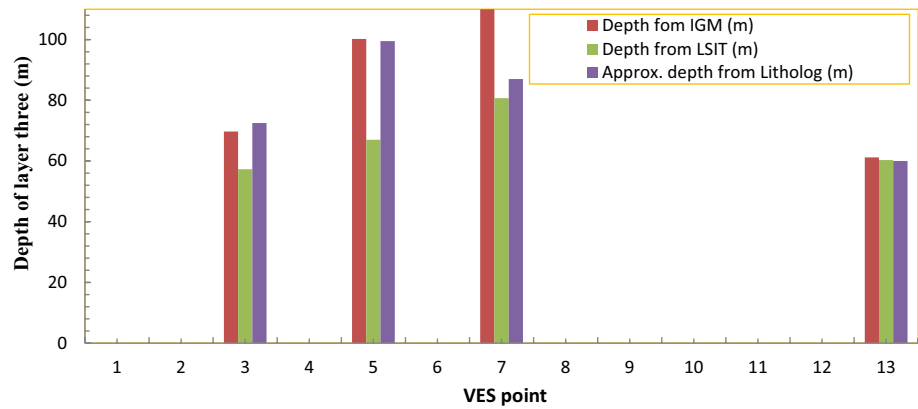


**Fig. 12** Delineated depth correlation of IGM and LSIT with approximate layer three depth from lithological data at different VES locations



Based on the modelled datasets obtained through ISM and LSIT modelling and the observed data from nearby borehole logs in the study area, model optimization were performed using depth parameter estimation schemes in model calibration. Using the expression in Eq. 6, the models obtained using ISM have 94%, 100% and 99% as the Nash–Sutcliffe optimization criterion model efficiency coefficients for layers 1–3, respectively. This shows excellent model according to Yao et al. (2007). The depth parameter estimation schemes in model calibration optimization criterion for LSIT according Eq. 6 also gives 99%, 100% and 96% as the percentage efficiency coefficient. This also implies excellent model as opined by Yao et al. (2007). The results of optimization as reflected by model error variance in both the scaled and re-scaled calibrations in Eqs. 5 and 6 show uniform optimization coefficients, reflecting excellent models of geologic units inferred using ISM and LSIT with respect to the observed geology. However, a novel observation indicates that the ISM is marginally better than LSIT based on the optimization indices realized in both the regression analyses and the Nash–Sutcliffe optimization criterion model.

## Conclusion

This work was undertaken to assess the efficiency of ISM and LSIT in-line with ground truthing indices. Geo-electrical resistivity technology employs these exploratory tools (ISM and LSIT) for explorability of groundwater and related subsurface resources related to archeology, engineering, mining and environment. The appraisal between the results obtained from inverse slope method (ISM) and the conventional digitally computerized least-squares inversion technique (LSIT) of geo-electrical resistivity data interpretation indicate that the geo-electrical models derived from ISM is practically more correlated to the borehole indices than the LSIT, which assumes regularization schemes or models for inverting the resistivity of the earth. The results show that the first layer resistivity values ranged from 67.6–2000.0  $\Omega\text{m}$  and 89.6–1464.2  $\Omega\text{m}$  with average values 2000.0  $\Omega\text{m}$  and 682.3  $\Omega\text{m}$ , respectively, for ISM and LSIT. The second layer resistivity ranged 384.6–3333.3  $\Omega\text{m}$  and 308.3–2591.8  $\Omega\text{m}$  with average 1467.0  $\Omega\text{m}$  and 1481.3  $\Omega\text{m}$  for ISM and

**Table 2** Ranges and averages of primary geo-electric indices determined from ISM and LSIT

Layer	Resistivity (Ohm-m) ISM		Resistivity (Ohm-m) LSIT		Thickness (m) ISM		Thickness (m) LIST		Depth (m) ISM		Depth (m) LSIT	
	Range	Average	Range	Average	Range	Average	Range	Average	Range	Average	Range	Average
1	67.6–2000.0	2000.0	89.6–1464.2	682.3	0.4–17.8	5.6	1.2–11.8	4.8	0.4–17.8	5.4	1.2–11.8	4.8
2	384.6–3333.3	1467.0	308.3–2591.8	1481.3	1.4–63.8	38.2	5.0–73.0	41.5	5.6–67.6	43.6	6.5–76.0	46.3
3	454.4–2500.0	1221.7	234.8–2301.8	1279.5	55.6–92.7	66.2	41.7–58.1	49.7	61.2–110.0	87.9	57.3–80.7	67.4
4	256.0–1666.7	836.3	542.2–1194.6	880.8	–	–	–	–	–	–	–	–

LSIT, respectively. Correspondingly, layer three interpreted by ISM and LSIT showed resistivity ranges of 454.4–2500.0  $\Omega\text{m}$  and 234.8–2301.8  $\Omega\text{m}$  with averages of 1221.7  $\Omega\text{m}$  and 1279.5  $\Omega\text{m}$  while the fourth layer is identified with resistivity spread from 256.0–1666.7  $\Omega\text{m}$  to 542.2–1194.6  $\Omega\text{m}$  with corresponding averages of 836.3  $\Omega\text{m}$  and 880.8  $\Omega\text{m}$ . Layer resistivity analysis indicates marginal correlation in layer one to maximal correlation of resistivities in layers two and three (Figs. 7, 8, and 9). Additionally, the curve types obtained from LSIT were 100% in agreement with the values of resistivity obtained for different layers in ISM. The depth of investigation showed that the LSIT showcased a correlation with borehole depth in the range of 56.3–88.6% (average: 70.3%) while ISM has average correlation of 79.0% with range of 68.0–87.7% in layers one to three distinctively delineated in this study. Based on the depth and thickness analyses displayed on Table 2 and Figs. 10, 11, and 12, ISM is more compliant with the drilling data than the conventional and digitally computerized method (LSIT). As conventionally known, LSIT is ill-posed problem that gives room for myriads of solutions based on interpreter's subjectivity to the interpretation of data acquired. ISM is advantageous as its quantitative results (the determination of the exact number of layers of the subsoil) and qualitative results (true resistivities, depths and thicknesses of the different layers) are linear and simpler than the logarithmic curve-matching of LSIT. A unit layer identified by curve-matching method due to problem of equivalence and suppression can be robustly resolved into two or more layers by ISM in some case studies as opined by Asfahani (2016). Incorporation of LSIT with ISM, which is more correlated with the available lithological ground truths than the currently used conventional method (LSIT) as revealed in this work, can reduce ambiguity and the non-uniqueness in VES interpretation mostly in areas where there is ground truthing information.

**Acknowledgements** We are thankful to our colleagues in Geophysics Research Group (GRG) of Akwa Ibom State University for their assistance during the field data acquisition and editing of the manuscript

**Funding** The project was funded by the authors.

## Declarations

**Conflict of interest** The authors declare that they have no known competing financial interests or personal relationships that could have appeared to influence the work reported in this paper.

**Human and animal rights** This article does not contain studies with human or animal subjects.

## References

- Akpan AE, Ugbaja AN, George NJ (2013) Integrated geophysical, geochemical and hydrogeological investigation of shallow groundwater resources in parts of the Ikom-Mamfe embayment and the adjoining areas in Cross River State Nigeria. *Environ Earth Sci* 70(3):1435–1456. <https://doi.org/10.1007/s12665-013-2232-3>
- Akpan AE, Ugbaja AN, Okoyeh EI, George NJ (2018) Assessment of spatial distribution of contaminants and their levels in soil and water resources of Calabar, Nigeria using geophysical and geological data. *Environ Earth Sci Ger* 77:13. <https://doi.org/10.1007/s12665-017-7189-1>
- AL-Hameedawi MM, Thabit JM, AL-Menshedv FH (2021) Some notes about three types of inhomogeneity and their effect on the electrical resistivity tomography data. *J App Geophys* 191:104360. <https://doi.org/10.1016/j.jappgeo.2021.104360>
- Asfahani J (2016) Inverse slope Method for interpreting vertical electrical soundings in sedimentary phosphatic environments in the Al-Sharquieh Mine, Syria. *CIM J* 7:30. <https://doi.org/10.15834/cimj.2016.12>
- Bandani E (2011) Application of groundwater mathematical model for assessing the effects of galoogah dam on the shooro aquifer-Iran. *Euro J Sci Res* 54(4):499–511
- Binley A, Ramirez A, Daily W (1995) Regularised image reconstruction of noisy Electrical resistivity tomography data. In: *Proceedings of the 4th Workshop of the European concerted action on process tomography*, Bergen, pp 401–410
- Bouadou RAM, Kouassi KA, Kouassi FW, Coulibaly A, Gnagne T (2019) Use of the inverse slope method for the characterization of geometry of basement aquifers: case of the department of boua (ivory coast). *J Geosci Env Prot* 7:166–183. <https://doi.org/10.4236/gep.2019.76014>
- Ekanem AM, George NJ, Thomas JE, Nathaniel EU (2019) Empirical relations between aquifer geohydraulic–geoelectric properties derived from surficial resistivity measurements in parts of Akwa Ibom state, Southern Nigeria. *Nat Resour Res*. <https://doi.org/10.1007/s11053-019-09606-1>
- Ekanem AM, Akpan AE, George NJ, Thomas JE (2021) Appraisal of protectivity and corrosivity of surficial hydrogeological units via

- geo-sounding measurements. *Environ Monit Assess.* <https://doi.org/10.1007/s10661-021-09518-9> (PMID: 34642861)
- Ekanem KR, George NJ, Ekanem AM (2022) Parametric characterization, protectivity and potentiality of shallow hydrogeological units of a medium-sized housing estate. *Acta Geophys, Shelter Afrique, Akwa Ibom State, Southern Nigeria.* <https://doi.org/10.1007/s11600-022-00737-3>
- Evans UF, George NJ (2007) Resistivity study of groundwater potential at Aka-Offot and Ikot Ntuen Nsit villages in Uyo capital city development area of Akwa Ibom State, Nigeria. *J Env Stud Nigeria* 3(4):114–118
- Friedel S (2003) (2003) Resolution, stability and efficiency of resistivity tomography estimated from a generalized inverse approach. *Geophys J Int* 153:305–316
- George NJ (2020) Appraisal of hydraulic flow units and factors of the dynamics and contamination of hydrogeological units in the littoral zones: a case study of Akwa Ibom State University and its environs, Mkpato Enin L.G.A Nigeria. *Nat Resour Res* 29:3771–3788. <https://doi.org/10.1007/s11053-020-09673->
- George NJ, Nathaniel EU, Etuk SE (2014) Assessment of economically accessible groundwater reserve and its protective capacity in Eastern Obolo local government area of Akwa Ibom State, Nigeria, using electrical resistivity method. *Int J Geophys* 2014:1–10. <https://doi.org/10.1155/2014/578981>
- George NJ, Emah JB, Ekong UN (2015) Geohydrodynamic properties of hydrogeological units in parts of Niger delta, southern Nigeria. *J Afr Earth Sc* 105:55–63. <https://doi.org/10.1016/j.jafrearsci.2015.02.009>
- George NJ, Ekanem AM, Ibanga JI, Udosen NI (2017) Hydrodynamic implications of aquifer quality index (AQI) and flow zone indicator (FZI) in groundwater abstraction: a case study of coastal hydro-lithofacies in south-eastern Nigeria. *J Coast Conserv* 21:759–776. <https://doi.org/10.1007/s11852-017-0535-3>
- George NJ, Ekanem AM, Thomas JE (2021) EkongSA (2021) Mapping depths of groundwater-level architecture: implications on modest groundwater-level declines and failures of boreholes in sedimentary environs. *Acta Geophys* 69:1919–1932. <https://doi.org/10.1007/s11600-021-00663-w>
- Ghanati R, Fallah Safari M (2021) DC Electrical resistance tomography inversion. *J Earth and Space Phys.* <https://doi.org/10.22059/jesphys.2021.323911.1007321>
- Ibanga Jewel I, George NJ (2016) Estimating geohydraulic parameters, protective strength, and corrosivity of hydrogeological units: a case study of ALSCON Ikot Abasi, southern Nigeria. *Arab J Geosci* 9(5):1–16
- Ibuot JC, Akpabio GT, George NJ (2013) A survey of the repository of groundwater potential and distribution using geo-electrical resistivity method in Itu local government area (L.G.A.), Akwa Ibom State, southern Nigeria. *Central Eur J Geosci* 5(4):538–547. <https://doi.org/10.2478/s13533-012-0152-5>
- Ibuot JC, George NJ, Okwesili AN, Obiora DN (2019) Investigation of litho-textural characteristics of aquifer in Nkanu West local government area of Enugu state, southeastern Nigeria. *J Afr Earth Sci Egypt* 153:197–207. <https://doi.org/10.1016/j.jafrearsci.2019.03.004>
- Ikpe EO, Ekanem AM, George NJ (2022) Modelling and assessing the protectivity of hydrogeological units using primary and secondary geo-electric indices: a case study of Ikot Ekpene urban and its environs, southern Nigeria. *Modeling Earth Sys Environ.* <https://doi.org/10.1007/s40808-022-01366-x>
- Kouassi FW, Kouassi KA, Coulibaly A, Kamagaté B, Savané I (2017) Efficiency of inverse slope method in the interpretation of electrical resistivity soundings data of schlumberger type. *Int J Eng Sci Res* 7(121):130
- Loke MH, Barker RD (1996) Rapid least-squares inversion of apparent resistivity pseudosections by a quasi-Newton method. *Geophys Prospect* 44:131–152
- Loke MH, Dalhin T (2002) A comparison of the Gauss-Newton and quasi-Newton methods in resistivity imaging inversion. *J App Geophys* 49:149–462
- Loke MH, Acworth I, Dalhin T (2003) A comparison of smooth and blocky inversion methods in 2-D electrical imaging surveys. *Explor Geophys* 34:182–187
- Mohamed HS, Senosy MM, Abdel Aal GZ (2014) Upgrading of the inverse slope method for quantitative interpretation of earth resistivity measurements. *Arab J Geosci* 7:4059–4077. <https://doi.org/10.1007/s12517-013-1075-2>
- Obinawu VI, George NJ, Udofia KM (2011) Estimation of Aquifer Hydraulic Conductivity and Effective Porosity Distributions using Laboratory Measurements on Core Samples in the Niger Delta, Southern Nigeria. *Int Rev Phys Praise Worthy Prize Italy* 5(1):19–24
- Obiora DN, Ibuot JC, George NJ (2015) Evaluation of aquifer potential, geoelectric and hydraulic parameters in Ezza North, southeastern Nigeria, using geoelectric sounding. *Int J Sci Technol.* <https://doi.org/10.1007/s13762-015-0886-y>
- Oladapo MI, Mohammed MZ, Adeoye OO, Adetola BA (2004) Geoelectrical investigation of the Ondo state housing corporation estate Ijapo Akure. *Southwestern Nigeria J Min Geol* 40(1):41–48
- Panda B, Chidambaram S, Ganesh N (2017) An attempt to understand the subsurface variation along the mountain front and riparian region through geophysics technique in South India. *Modeling Earth Syst Environ* 3(2):783–797. <https://doi.org/10.1007/s40808-017-0334-8>
- Petters SW (1982) Central West African cretaceous: tertiary benthic foraminifera and stratigraphy. *Palaeontograph A* 179:1–104
- Petters SW (1989) Akwa Ibom State: physical background, soil and land use and ecological problems. Technical report for government of Akwa Ibom State, p 603
- Sanjiv KS (2010) Site characterization studies using electrical resistivity technique in Gudwanwadi dam site, Karjat, Maharashtra (p. 47). Master of science in applied geophysics, Bombay: department of earth science indian institute of technology
- Sankarnaryan PV, Ramanujachary KR (1967) An inverse slope method for determining absolute resistivities. *Geophysics* 32(6):1036–1040
- Short KC, Stäuble AJ (1965) Outline of geology of Niger delta. *Am Asso Petrol Geol Bull* 51:761–779
- Simms JE, Morgan FD (1992) Comparison of four least-squares inversion schemes for studying equivalence in one-dimensional resistivity interpretation. *Geophysics* 57:1282–1293
- Temitope OAA, JA, (2016) Geophysical characterization of aquifer parameters within basement complex rocks using electrical sounding data from the polytechnic, Ibadan, Southwestern Nigeria. *Int J Sci Res* 4:112–127. <https://doi.org/10.12983/ijsrk-2016-p0112-0127>
- Thomas JE, George NJ, Ekanem AM, Nsikak EE (2020) Electrostratigraphy and hydrogeochemistry of hyporheic zone and water-bearing caches in the littoral shorefront of Akwa Ibom State university, southern Nigeria. *Environ Monit Assess* 192:505. <https://doi.org/10.1007/s10661-020-08436-6>
- Tizro AT, Voudouris K, Basami Y (2012) Estimation of porosity and specific yield by application of geoelectrical method: a case study in western Iran. *J Hydrol* 454–455:160–172. <https://doi.org/10.1016/j.jhydrol.2012.06.009>
- Tripp AC, Hohmann GW, Swift CM Jr (1984) Two-dimensional resistivity inversion. *Geophysics* 49(10):1708–1717
- Udosen NI, George NJ (2018a) A finite integration forward solver and a domain search reconstruction solver for electrical resistivity



- tomography (ERT). *Model Earth Syst Environ* 4:1–12. <https://doi.org/10.1007/s40808-018-0412-6>
- Udosen NI, George NJ (2018b) Characterization of electrical anisotropy in north Yorkshire England using square arrays and electrical resistivity tomography. *Geomech Geophys Geo-Energy Geo-Resour* 4(3):215–233. <https://doi.org/10.1007/s40948-018-0087-5>
- Uwa UE, Akpabio GT, George NJ (2019) Geohydrodynamic parameters and their implications on the coastal conservation: a case study of Abak local government area (LGA), Akwa Ibom State, southern Nigeria. *Nat Resour Res* 28(2):349–367. <https://doi.org/10.1007/s11053-018-9391-6>
- Vander Velpen BPA, Sporry RJ (1993) Resist: a computer program to process resistivity sounding data on PC compatibles. *Comput Geosci* 19(5):691–703
- Yao BK, Lasm T, Ayrat PA, Johannet A, Kouassi AM, Assidjo E, Biémi J (2007) Optimisation des modèles Perceptrons Multicouches avec les algorithmes de premier et de deuxième ordre. application à la modélisation de la relation plu-ie-débit du Bandama Blanc, Nord de la Côte d’Ivoire. *Eur J Sci Res* 17:13–328
- Zohdy AAR (1989) A new method for automatic interpretation of Schlumberger and Wenner sounding curves. *Geophysics* 5(2):245–252
- Zohdy AAR, Eaton GP, Mabey DR (1974) Application of surface geophysics to groundwater investigations. US geological survey techniques of water-resources investigations, Book 2. p 116 Chapter D1